Friction **12**(4): 606–617 (2024)
https://doi.org/10.1007/s40544-023-0763-5
ISSN 2223-7690
CN 10-1237/TH
RESEARCH ARTICLE

Adsorption limitation investigation on olefins for Cu–BTC

Xiao YANG[1,2,*], Yunbo WANG[1,2], Weihua CAO[1,2], Ruizheng JIANG[1,2], Guoxin XIE[3,*], Yuying CAO[1], Xiaowen QI[1,4]

[1] *School of Mechanical Engineering, Yanshan University, Qinhuangdao 066004, China*

[2] *Key Laboratory of Self-Lubricating Spherical Plain Bearing Technology of Hebei Province, Yanshan University, Qinhuangdao 066004, China*

[3] *State Key Laboratory of Tribology in Advanced Equipment, Department of Mechanical Engineering, Tsinghua University, Beijing 100084, China*

[4] *Aviation Key Laboratory of Science and Technology on Generic Technology of Self-Lubricating Spherical Plain Bearing, Yanshan University, Qinhuangdao 066004, China*

Received: 26 August 2022 / Revised: 16 November 2022 / Accepted: 21 March 2023

Abstract: To utilize Cu–benzene-1,3,5-tricarboxylate (Cu–BTC) adsorbed lubricant oils in the self-lubricating field, the adsorption properties of Cu–BTC on different 1-olefins must be clarified. In this work, 1-hexene, 1-octene, 1-nonene, 1-decene, 1-undecene, and 1-dodecene were studied by the Monte Carlo method and experimentally. The adsorption limit of Cu–BTC for n-olefins was determined as 1-undecene by the adsorption isotherms. This suggested a limit for even straight-chain molecules to the adsorption of Cu–BTC. The maximum ratio of the olefin length of the largest pore diameter (*L*/*D*) of Cu–BTC was approximately 1.57. Furthermore, theoretical calculations (radial distribution function (RDF)) and experiments (infrared (IR) spectra) confirmed the interaction of n-olefin adsorbates and the Cu–BTC framework occurred between the –CH= of olefins and the Cu and O atoms of the Cu–BTC framework. This work adds to the understanding and investigation of the adsorption of liquid lubricants using Cu–BTC as a metal–organic framework (MOF).

Keywords: metal–organic framework (MOF); Cu–benzene-1,3,5-tricarboxylate (Cu–BTC); Monte Carlo method; adsorption properties; 1-olefins

1 Introduction

A metal–organic framework (MOF) is an organic–inorganic hybrid crystalline compound, in which metal ions or clusters bond with organic linkers (divalent or trivalent aromatic carboxylic acids or azoles) to form a solid porous periodic framework [1, 2]. It is an important member of the porous material family due to its high porosity, large surface area, controllable porous structure, and variety of chemical components [3–7]. The MOF has seen extensive use in catalysis, gas separation, and drug delivery due to its high porosity [8–11]. Furthermore, two-dimensional (2D) MOF structures have become ideal materials for solid super sliding due to their benefits in molecular-level structure and regulation [12, 13]. Reference [14] incorporated a three-dimensional (3D) porous MOF of Cu–benzene-1,3,5-tricarboxylate (Cu–BTC) with an oil amine into a resin matrix as a lubricant, which demonstrated ultra-low friction and suggested the use of MOFs as self-lubricating materials. Obviously, an oil amine adsorbed by Cu–BTC participates and lowers the coefficient of friction (CoF). This differed from widely used metals and other composite materials with solid lubricant nanoparticles. Traditionally, the nanoparticles incorporated as solid lubricants into fluids tended to agglomerate, which led to the necessity of surface functionalization [15–17].

* Corresponding authors: Xiao YANG, E-mail: yxiao.ysu@hotmail.com; Guoxin XIE, E-mail: xgx2014@tsinghua.edu.cn

Self-lubricating composite materials, the nanoparticles of solid lubricants incorporated into materials, have solved this problem well [18, 19]. Metal matrix self-lubricating composites are obtained by sintering metal powders and meeting specific requirements through process control [20]. However, important factors like matrix characteristics, nanophase volume percentage, nanophase size, nanophase morphology, matrix–nanophase interface, and various environmental parameters impacted the CoF and wear rates of metal matrix nanocomposites (MMNCs), irreplaceable materials in tribology industries [21]. This differed from self-lubricating materials that contained MOF nanocontainers. The lubrication mode of MOFs in 2D layers approximated solid lubricants (e.g., MoS_2, graphene, etc.). But 3D porous MOF materials can adsorb liquid lubricants. MOFs containing lubricants were added to the base material to form self-lubricating materials, which have the advantages of intelligent adsorption/release and recycling, as compared to self-lubricating composites with solid nanoparticles. Squeezing the base material during friction released the lubricant, which can adsorb back into the frame upon load removal. The study on Cu–BTC did not clarify whether the adsorption of the oil amine occurred by surface adsorption or internal adsorption. To the best of our knowledge, few studies examining whether porous MOFs can adsorb lubricating oils into their framework pores, the adsorption mechanism, and capacity during absorption have been reported.

Among various MOFs, Cu–BTC[$Cu_3(BTC)_2(H_2O)_3$], first reported by Chui et al. [22] in 1999, is one of the more common and well-studied MOFs. Cu–BTC pores comprise a main channel with a square cross-section (~9 Å) and eight tetrahedral side bags (5 Å) [23], which intersect to form a 3D pore network with a simple cubic symmetry. There have been various computer simulations on hydrocarbon adsorptions by Cu–BTC [24, 25], but most Cu–BTC research focused mainly on its adsorption and separation of light hydrocarbons (number of carbon atoms $\leqslant 4$) [26–28]. Klein et al. [29] measured the adsorption of butane by Cu–BTC and found the butane concentration related to its adsorption capacity. Lamia et al. [30], Jorge et al. [31], and Rubeš et al. [32] studied propane/propylene separation and isobutene adsorption. Due to the Cu bond, propylene had strong interactions with the unsaturated metal sites, which promoted adsorption. These interactions also significantly improved the affinity of Cu–BTC for unsaturated hydrocarbons. Van Assche et al. [33] studied the adsorption of polar and non-polar molecules on Cu–BTC and found that Cu–BTC adsorbed polar or non-polar molecules equally well. For small polar molecules, the two cages of Cu–BTC showed different adsorption mechanisms and two-step adsorption behavior. They also found that water exposure reduced the adsorption properties of the Cu–BTC framework. For the Cu–BTC simulation, Ref. [34] mainly focused on saturated hydrocarbons. Chmelik et al. [35] studied the adsorption and diffusion of n-butane, isobutane, 2-methyl butane, and 2,2-dimethylpropane in Cu–BTC by using an infrared (IR) microscope and a molecular simulation. Cu–BTC adsorbed fewer C_4H_{10} and C_5H_{12} alkanes than C_2H_6 alkanes under the same load, which implied that the adsorption capacity correlated negatively with the molecular size. However, the adsorption performance of Cu–BTC with long-chain olefins, especially the maximum adsorbable olefin, remains unclear.

This work studied the adsorption performance of Cu–BTC with long-chain normal olefins (number of C atoms > 4). The adsorption limit of Cu–BTC for olefins occurred using 1-undecene. The maximum ratio of olefin length (L) to the larger pore diameter (D) of Cu–BTC (L/D; approximately 1.57) suggested the adsorption limitation for Cu–BTC. The interactions between the olefins and the Cu–BTC framework occurred with –CH= of olefins and the Cu and O atoms of Cu–BTC. This work provides theoretical support for the adsorption and desorption of liquid lubricants on Cu–BTC-like MOFs.

2 Test method

2.1 Molecular dynamics (MD) simulations

Cu–BTC is an MOF material with a metal Cu ion as a node and a trichloromethyl chain as a skeleton (its lattice structure is shown in Fig. 1(a)). There are two pores in the cell with diameters of 9 and 5 Å. Figure 1(b) shows a 3D view of the Cu–BTC material supercell structure. The Cu–BTC is a porous material that contains many channels and pores on each surface.

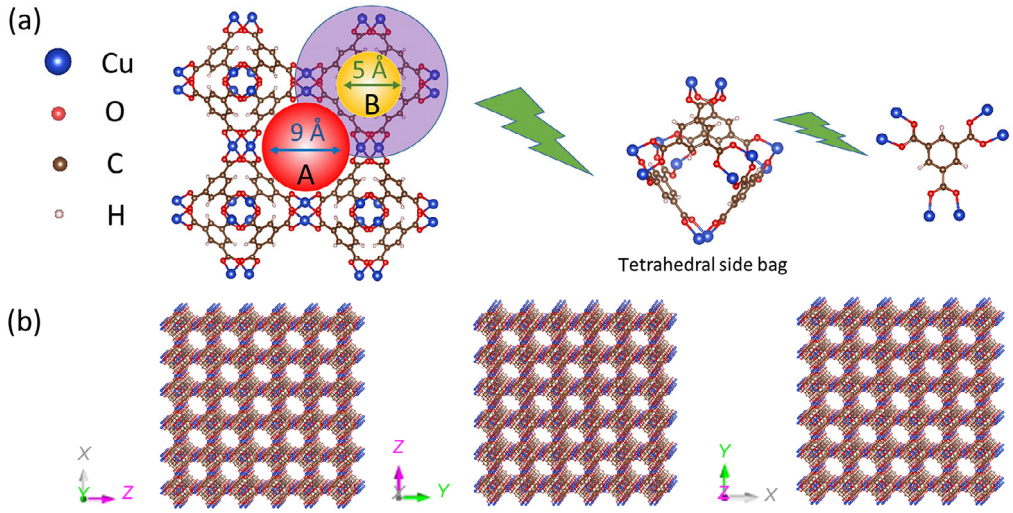

Fig. 1 (a) Cu–BTC and its single-cell organic chain structure and (b) 3D view of Cu–BTC crystal structure.

Figure 2 shows the molecular structures of 1-hexene, 1-octene, 1-nonene, 1-decene, 1-undecene, and 1-dodecene and are labelled as C6, C8, C9, C10, C11, and C12, respectively. The molecular chain lengths are 9.255, 10.470, 11.685, 12.917, 14.115, and 15.340 Å, respectively, larger than those of the two voids in the Cu–BTC structure.

This work adopted a DFT molecular force field developed by Kulkarni and Sholl [36], which accurately describes the adsorption law of olefin or kerosene molecules in Cu–BTC. Figure 3 shows the adsorption isotherms of Cu–BTC for propylene under different pressures and temperatures; the curve represents the calculation results, and the data points represent the experimental results [36]. The adsorption results using this molecular force field and potential function agreed with the experimental results.

2.2 Calculation settings

Grand-canonical Monte Carlo (GCMC) simulations calculated the adsorption isotherms using the RASPA [37] simulation code; a configurational bias method was introduced to the Monte Carlo sample. The adsorption isotherms of Cu–BTC with long-chain olefin molecules were calculated, keeping the Cu–BTC structure rigid and the 1-olefins flexible. A 2 × 2 × 2 Cu–BTC supercell was used in the calculation, and the pairwise interaction between atoms was truncated at the spherical cross-section wave at a diameter of 13.0 Å. The Monte Carlo moves included molecular translation, rotation, regrowth at a random position, insertion, and deletion as well as identity changes in the case of mixtures. For the long-range dispersion interaction simulation, an analytical tail correction was included. Firstly, 100,000 configurational bias

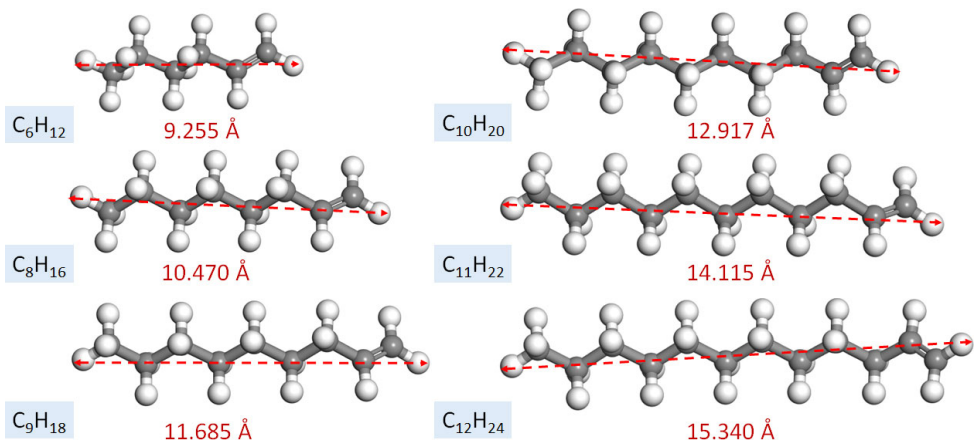

Fig. 2 Molecular structures of adsorbates: 1-hexene, 1-octene, 1-nonene, 1-decene, 1-undecene, and 1-dodecene.

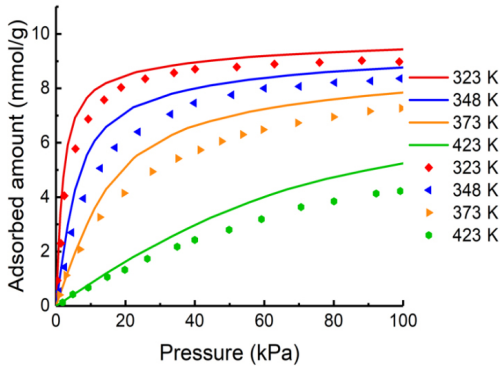

Fig. 3 Comparison of calculated (the curves) and experimental (the points) adsorption isotherms of propylene after potential function optimization. Reproduced with permission from Ref. [36], © American Chemical Society 2016.

Monte Carlo (CBMC) cycle calculations were optimized, followed by 400,000 calculation cycles to determine the adsorption performance of the system. The interaction between Cu and each atom in the olefin molecule was expressed by the Morse simple harmonic molecular force field.

3 Adsorption experiments

3.1 Material purchase

All chemicals were purchased from commercial sources and used without further purification: 1-hexene (99%, Aladdin Reagent Co., Ltd.), 1-heptene (98%, Aladdin Reagent Co., Ltd.), 1-octene (98%, Shanghai Meiruier Chemical Technology Co., Ltd.), 1-nonene (95%, Beijing Inokai Technology Co., Ltd.), 1-decene (95%, Aladdin Reagent Co., Ltd.), 1-undecene (98%, Aladdin Reagent Co., Ltd.), and Cu–BTC (particle size: 100 nm–3.5 μm, Nanjing Xianfeng Nano Technology Co., Ltd.).

3.2 Instruments and test methods

The Fourier transform IR (FTIR) spectra of Cu–BTC before and after adsorption were measured by an FTIR spectrometer (Nicolet IS5, Thermo Fisher, USA) from 4,000 to 500 cm^{-1}. The thermogravimetric (TG) measurements were made using a TG analyzer (STA449C, NETZSCH, Germany). The temperature was measured under nitrogen from 0–500 °C at a rate of 10 °C/min. The powder X-ray diffraction (XRD) patterns of fresh and adsorbed Cu–BTC were detected at room temperature on an X-ray diffractometer (D/MAX-2500/PC, Rigaku, Japan) using Cu Kα radiation (λ = 1.5406 Å) with a 2θ step of 0.02°, and 5 (°)/min from 5° to 50°.

3.3 Adsorption experiments

The dry Cu–BTC powder (0.2 g) was soaked and stirred in 3 mL of 1-hexene in a 5 mL of reagent bottle. After sealing, the mixture remained at room temperature (25 °C) for 3 d and thoroughly shaken every day. After adsorption, the mixture was placed in a vacuum oven at 50 °C for 24 h to completely dry the adsorbed Cu–BTC. This was repeated three times to yield the average adsorption capacity (mg/g). The adsorbed olefins (C6–C12) were labeled as LC6–LC12 (25 °C) and HC6–HC12 (50 °C; Fig. 4).

3.4 Friction experiments

The friction tests were conducted on the surfaces of iron sheets. Before testing, the iron sheets were ultrasonically cleaned (DS-2510DTH, Shanghai Shengfa Ultrasonic Instrument Co., Ltd., China) for 10 min, and white corundum deposited on the surface. Then 0.02 g of Cu–BTC samples were uniformly distributed on the processed iron sheet surfaces and tested for 30 min under a 3 N of load and 8 mm of dimension. A CSM friction and wear tester (Antonpa, CSM Instrument Co., Ltd., Switzerland) was used for the friction tests.

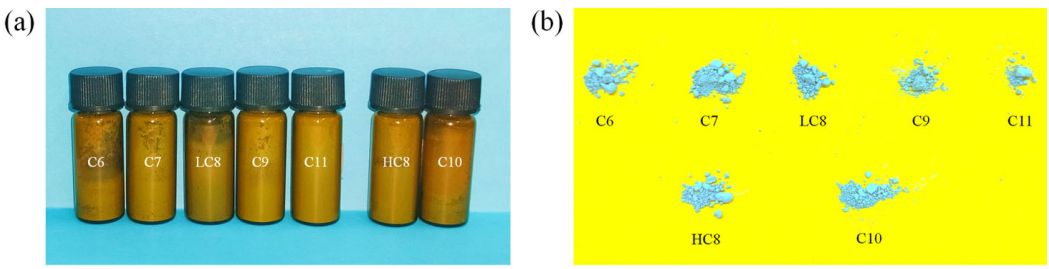

Fig. 4 Samples for adsorption experiments: (a) labels and (b) olefin-adsorbed Cu–BTC.

4 Results and discussion

4.1 MD simulation of Cu–BTC adsorption on different long-chain olefins

Figure 5(a) shows the adsorption isotherms of Cu–BTC for C6, C8, C9, C11, and C12 at 298 K. As shown in Fig. 5(a), the adsorption isotherms of these alkenes (except C12) followed a Langmuir pattern, consistent with the adsorption of pentane and argon by Cu–BTC [34]. The adsorption capacities were stabilized at 6.107, 4.344, 3.778, and 2.962 mmol/g for C6, C8, C9, and C11, respectively. For C12, the adsorption capacities were extremely low at any pressure.

Figure 5(b) shows the adsorption isotherms of Cu–BTC for C8, C10, and C12 under various pressures at 323 K. The adsorption capacity of C8 stabilized at 4.118 mmol/g as the pressure increased and was lower than that at 298 K. Temperature increases the enhanced thermal vibrations, weakened the interaction between the adsorption site and the adsorbates, and lowered the adsorption capacity of C8. The adsorption capacity of C10 was 3.154 mmol/g, though, for C12, the adsorption capacity was only 0.038 mmol/g (similar to that at 298 K), which implied that increasing the temperature had no effect on the adsorption of Cu–BTC with 1-dodecene.

The maximum adsorption capacities and step adsorption pressures for 1-hexene (C6), 1-octene (C8), 1-nonene (C9), 1-undecene (C11), and 1-dodecene (C12) are extracted (Fig. 6(a)) to study the effect of the number of carbons in Cu–BTC. Those results showed that the adsorption capacity decreased as the number of carbon atoms increased from 6 to 11 but decreased rapidly for C12 (to nearly 0 mmol/g). For the step adsorption pressure, it showed a nonlinear decrease with additional carbon atoms. The specific surface area of Cu–BTC, the relative pore sizes, and adsorbate molecules of Cu–BTC may impact its adsorption effect. The pore diameter ratio parameter L/D describes the relative size of olefin molecular length and pore diameter. Figure 6(b) shows the relationship between the maximum adsorption capacity of olefin molecules and the L/D ratio of Cu–BTC. The

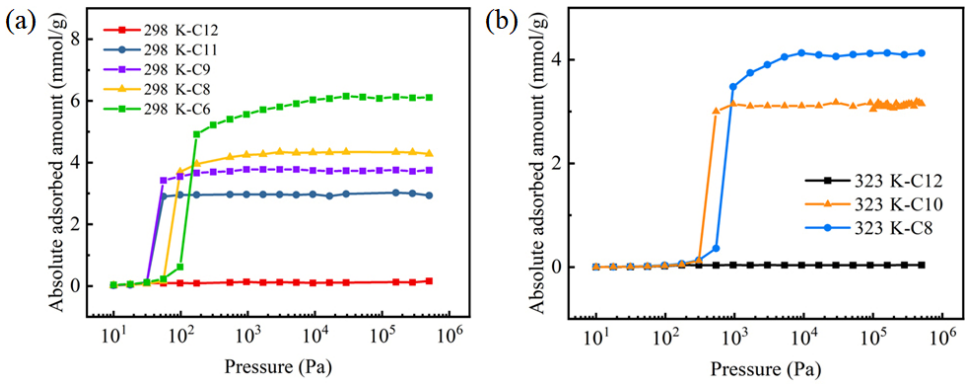

Fig. 5 Adsorption isotherms of different alkenes at (a) 298 and (b) 323 K.

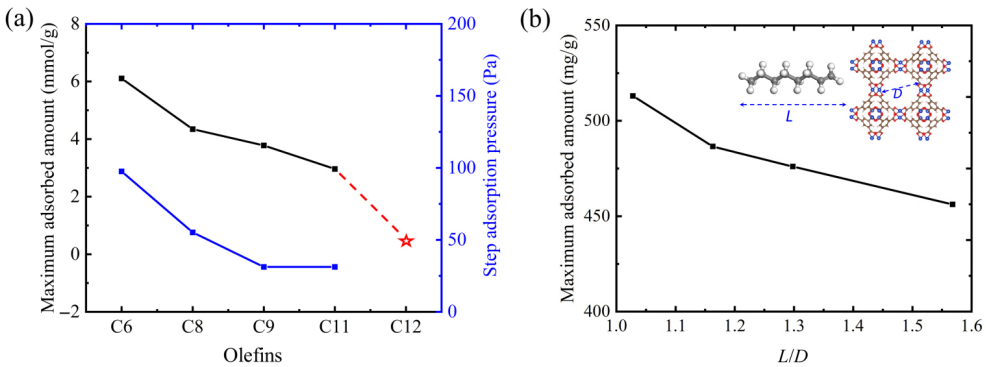

Fig. 6 Different long-chain olefins at 298 K: (a) Cu–BTC maximum adsorption capacities and step adsorption pressures and (b) relationship between maximum adsorption capacity and L/D (the insets show the L and D).

adsorption capacities of Cu–BTC towards adsorbable olefin molecules initially decreased rapidly from 1.03 to 1.15 of *L*/*D*, and then decreased linearly with additional *L*/*D* increases. The maximum adsorbable *L*/*D* was ~1.57.

Figure 7 compares the adsorption densities of C8 and C11 in different pores at 298 and 323 K. For C8, the adsorbed molecules localized more in the macropores at higher temperatures. For C11, the adsorption density was also more localized at higher temperatures, but the distribution localization was less obvious due to the molecular size difference.

4.2 Interaction between Cu–BTC and olefins

The radial distribution function (RDF) of Cu–BTC absorption of 1-octene was calculated at 298 K and 1 atm to study the Cu–BTC absorption characteristics (Figs. 8(a) and 8(b)). According to the RDF, the adsorption distance of Cu–CH was 2.62 Å, lower than the van der Waals radii sum of Cu and C atoms (3.13 Å), which indicated chemical adsorption. The adsorption distance of O–CH is 3.30 Å, slightly larger than the van der Waals radii sum of O and C atoms (3.22 Å), which suggested that adsorption may occur physically via van der Waals forces. In the RDF, the interaction between Cu and O for Cu–BTC with CH_2= for 1-octene always lagged –CH= (~0.95 Å). This analysis led us to conclude that olefins interact with target atoms during adsorption in the following ways: –CH= interacts with target atoms, CH_2=, and the remaining molecular segments randomly distribute in the voids following the principle of the minimum energy, as shown in Fig. 8(c).

The samples were tested by the IR spectra to analyze the interactions between olefins and Cu–BTC during adsorption; those results are shown in Fig. 9. The stretching vibration peaks at 3,454 cm^{-1} from –OH, benzene ring skeleton stretching vibrations peaks near 1,500 cm^{-1}, and benzene ring C–H bending vibration absorption peaks at 1,115 cm^{-1} were present

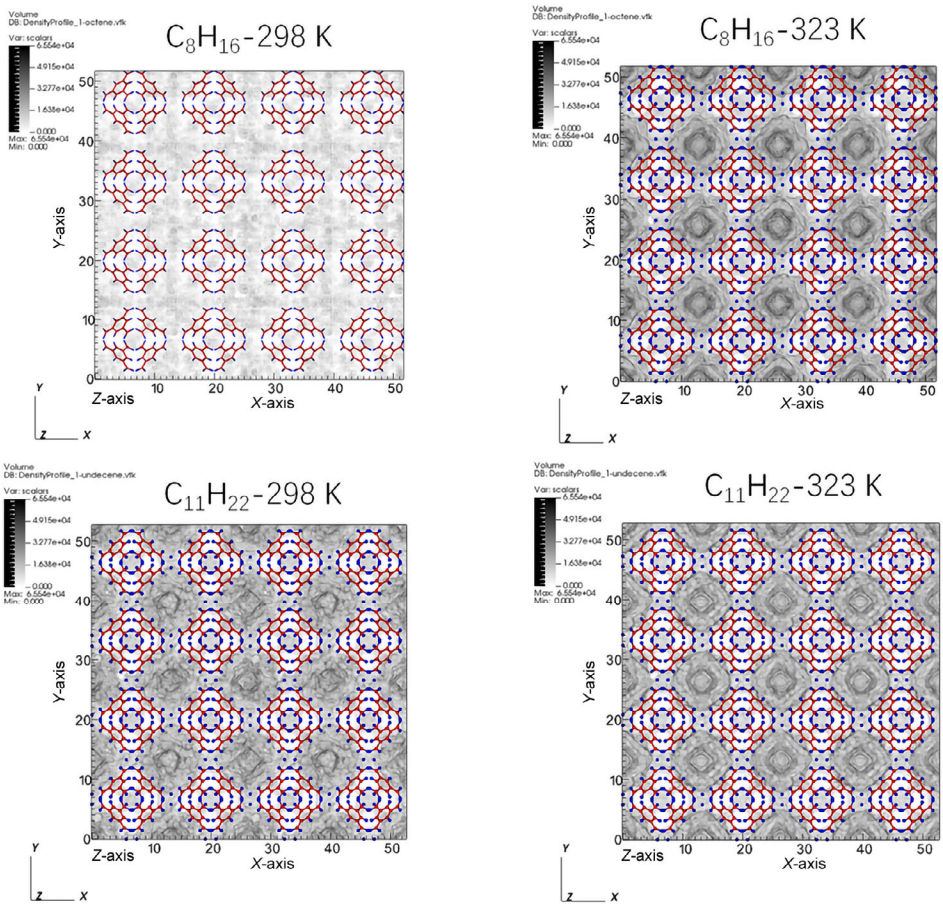

Fig. 7 Distributions of adsorption densities of Cu–BTC on 1-octene (C_8H_{16}) and 1-undecene ($C_{11}H_{22}$).

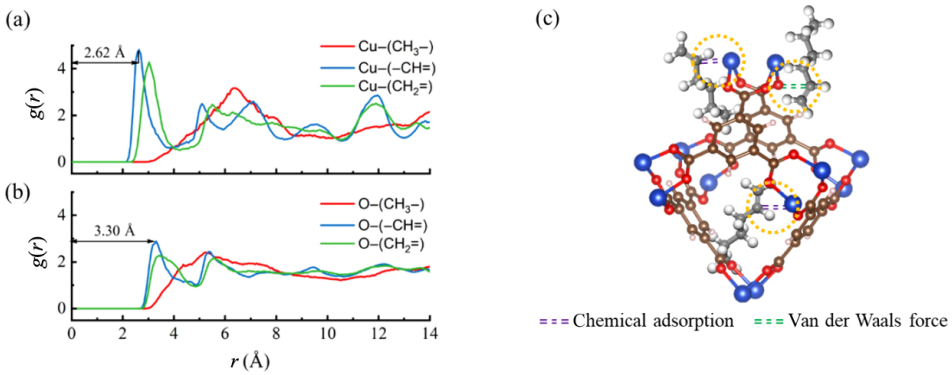

Fig. 8 RDF of Cu–BTC adsorbing 1-octene (C_8H_{16}) at 298 K and 1 atm, where (a) represents Cu atoms, and (b) represents O atoms and (c) sketch of 1-hexene mechanism on Cu–BTC. $g(r)$ refers to the ratio between the probability density of another particle appearing at the distance r from the center particle and the random distribution density.

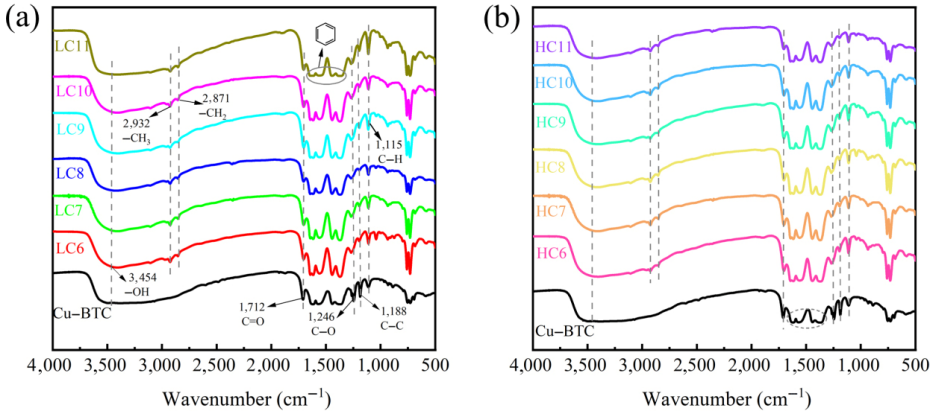

Fig. 9 FTIR spectra of Cu–BTC before and after olefin adsorptions at (a) 25 and (b) 50 °C.

both before and after adsorption. After adsorption, stretching vibrations of $–CH_3$ and $–CH_2$ appeared at 2,932 and 2,871 cm^{-1}, respectively, which indicated olefin adsorption by Cu–BTC. The characteristic peaks of C=O, C–O, and C–C at 1,712, 1,246, and 1,188 cm^{-1}, respectively, were inhibited, which indicated that olefins were adsorbed near COO– and inhibited vibrations from those functional groups and corresponded to one of the adsorption site of O atoms analyzed in the simulation.

Figure 10 represents the XRD patterns of pure and olefin-adsorbed Cu–BTC; characteristic peaks appeared at 2θ = 5.9°, 6.8°, and 9.5°, which corresponded to the (111), (200), and (220) crystal planes, respectively. The adsorbed Cu–BTC showed enhanced intensities of the characteristic peaks (2θ = 5.9° and 6.8°) and a smaller diffraction angle of the characteristic peak (2θ = 9.5°), which indicated that the adsorption distribution and adsorption of olefins in the framework increased the Cu–BTC lattice constant.

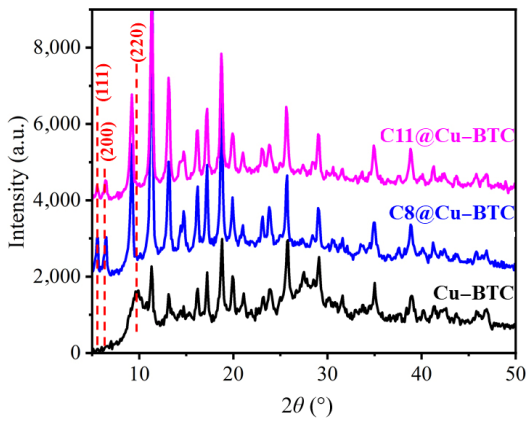

Fig. 10 XRD patterns of Cu–BTC before and after olefin adsorption.

4.3 Adsorption experiments of Cu–BTC on different long-chain olefins

Figure 11 shows the TG curves of Cu–BTC adsorbing different olefins; there were three weight loss steps during the heating. The desorption of water and

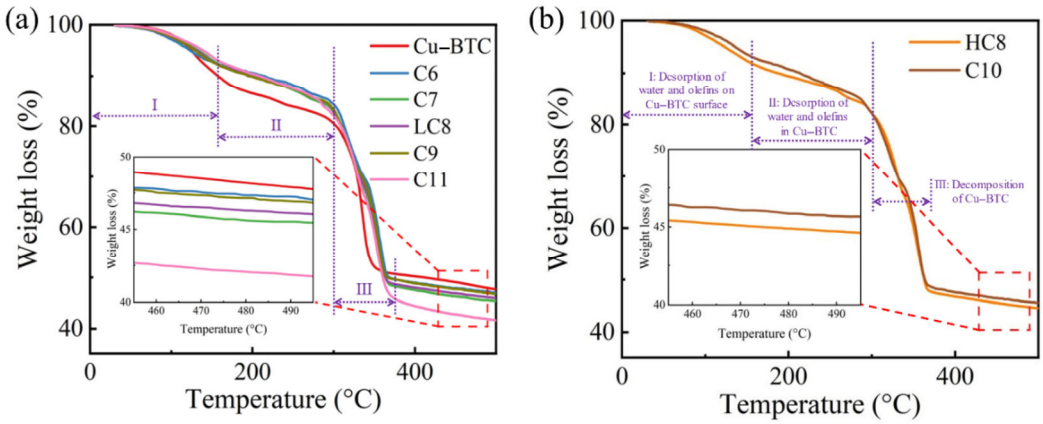

Fig. 11 TG curves of Cu–BTC adsorbing different olefins: (a) 25 and (b) 50 °C.

olefins on the surface of Cu–BTC occurred between 0 and 160 °C, while from 160 to 300 °C, water and olefins bound to the organic skeleton of Cu–BTC began to desorb. At 300–350 °C, the organic skeleton began to decompose and was unstable above 370 °C. Clearly, the TG curves for the olefins nearly overlap in the three stages. This was because Cu–BTC adsorbs less (mmol/g) of longer-chain 1-olefins, as suggested in Fig. 6(a). However, the longer 1-olefins obtain a higher molecular weight, so the molecular adsorption weight and amount achieve a balance. Therefore, even though the temperature change drives large differences in the adsorptions of 1-olefins, the adsorption weights are similar.

We calculated the thermal weight loss ratio, the thermal weight loss percentage of stage II (Fig. 11; 160–300 °C) divided by that in stage III (300–370 °C), and the experimental adsorption mass (mg/g) of Cu–BTC for olefins at 25 and 50 °C (Fig. 12). The thermal weight loss ratio views the internal adsorption quantity from the TG tests, the ratio of internal adsorbed molecules from the Cu–BTC. During the experiments, we discovered that olefin carbon content mirrored the adsorption quality. This suggested reliable adsorption experimental results.

The macro adsorption experimental results were compared with the simulation results at 25 and 50 °C (Table 1) and were in good agreement. Adsorption decreased with longer olefin chains, and the experimental adsorption capacities were slightly lower than the simulation results, which may be due to water adsorption during the macro experiment [33].

4.4 Tribology tests of Cu–BTC and olefin-adsorbed Cu–BTC

Pure Cu–BTC and olefin-adsorbed Cu–BTC were added to the iron sheet surface for a tribology test, as shown in Fig. 13. Those results showed that the CoF of olefin-adsorbed Cu–BTC was lower than that of the non-adsorbed initially, which indicated that the adsorbed olefins were extruded from the Cu–BTC framework and played a role as lubricants. With longer

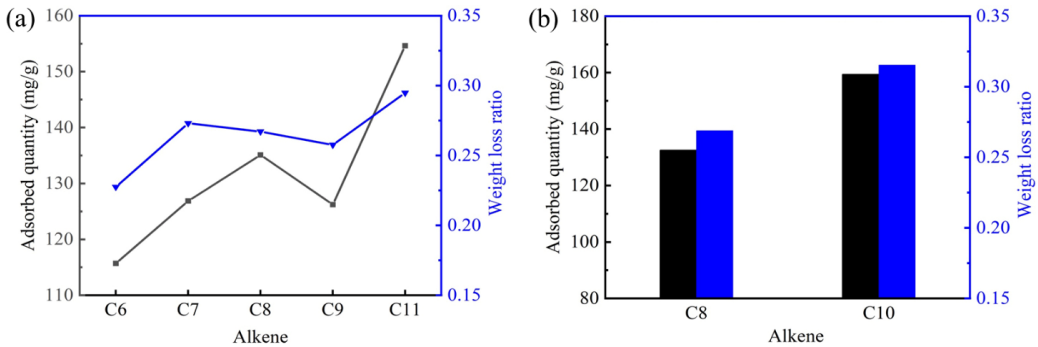

Fig. 12 Relationships between thermal weight loss (160–500 ℃) and olefin carbon content after Cu–BTC adsorbed different olefins at (a) 25 and (b) 50 °C.

Table 1 Comparison of experimental adsorption and simulated adsorption.

Temperature (°C)	Alkene	Experimental adsorption quality (mg/g)	Experimental adsorption amount (mmol/g)	Simulated adsorption amount (mmol/g)
25	C6	115.6934	1.3773	6.107
	C7	126.8701	1.2946	—
	C8	135.0906	1.2062	4.343
	C9	126.2152	1.0722	3.778
	C10	149.3716	1.0669	—
	C11	154.6253	1.0041	2.962
50	C6	117.6076	1.4001	—
	C7	125.3126	1.2787	—
	C8	138.5529	1.2371	4.127
	C9	143.9866	1.1428	—
	C10	159.4059	1.1386	3.153
	C11	156.0522	1.0133	—

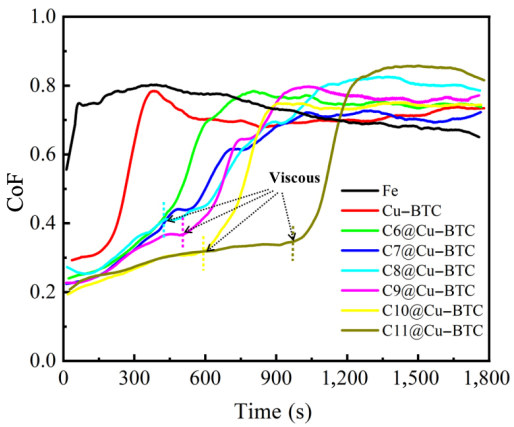

Fig. 13 CoF curves of non-adsorbed Cu–BTC and various olefin-adsorbed Cu–BTC.

friction time, shorter-chain olefins were consumed due to lower boiling points, and longer-chain olefins showed better lubrication effects. As the extruded olefins are viscous, a large amount of wear debris adhered to the Cu–BTC frame surface, which increased the CoFs. The olefins with longer carbon chains were more viscous and stable, the effect of wear debris adhesion was more obvious, and the CoF at the adhesion stage was higher.

Figure 14 shows the worn sample surfaces. The rough surface and gullies of the iron friction pair caused high CoF values, as shown in Fig. 14(a). The added Cu–BTC filled the interface gullies, but the wear particles in the smooth area also increased the wear rate, as shown in Fig. 14(b). Two compounds (1-hexene and 1-heptene) rapidly completed lubrication, adhesion, and volatilization; slight pitting corrosion occurred on the surface, as shown in Figs. 14(c) and 14(d). Two longer compounds (1-octene and 1-nonene) were relatively difficult to consume, and the friction pair was seriously damaged after adhesion, as shown in Figs. 14(e) and 14(f). The longest compounds (1-decene and 1-undecene) were stable at the friction pair interface with a lasting lubrication effect, as shown in Figs. 14(g) and 14(h). The accumulation of wear debris was quite evident, and the surface of the friction pair would degrade more significantly with continued testing.

5 Conclusions

The adsorption characteristics of the porous Cu–BTC MOF material for long-chain alkenes (1-hexene, 1-octene, 1-nonene, 1-undecene, and 1-dodecene) were studied and shown.

1) The adsorption limit of Cu–BTC for long-chain olefins was 1-undecene. Its *L*/*D* was ~1.57.

2) Olefin molecules adsorbed into two pores of the Cu–BTC framework structure.

3) Adsorption occurred on Cu and O atoms of Cu–BTC and interacted with olefin –CH= groups.

This work provides theoretical support for the adsorption and desorption of liquid lubricants on Cu–BTC and contributes to the understanding of the adsorption of liquid lubricants on other MOFs.

Acknowledgements

The National Natural Science Foundation of China (Grant No. 51905297), Natural Science Foundation of Hebei Province of China (Grant No. E2021203092), and the Opening Foundation of State Key Laboratory of Tribology, Tsinghua University (Grant No. SKLTKF21B13) are acknowledged.

Declaration of competing interest

The authors have no competing interests to declare that are relevant to the content of this article. The author Guoxin XIE is the Editorial Board Member of this journal.

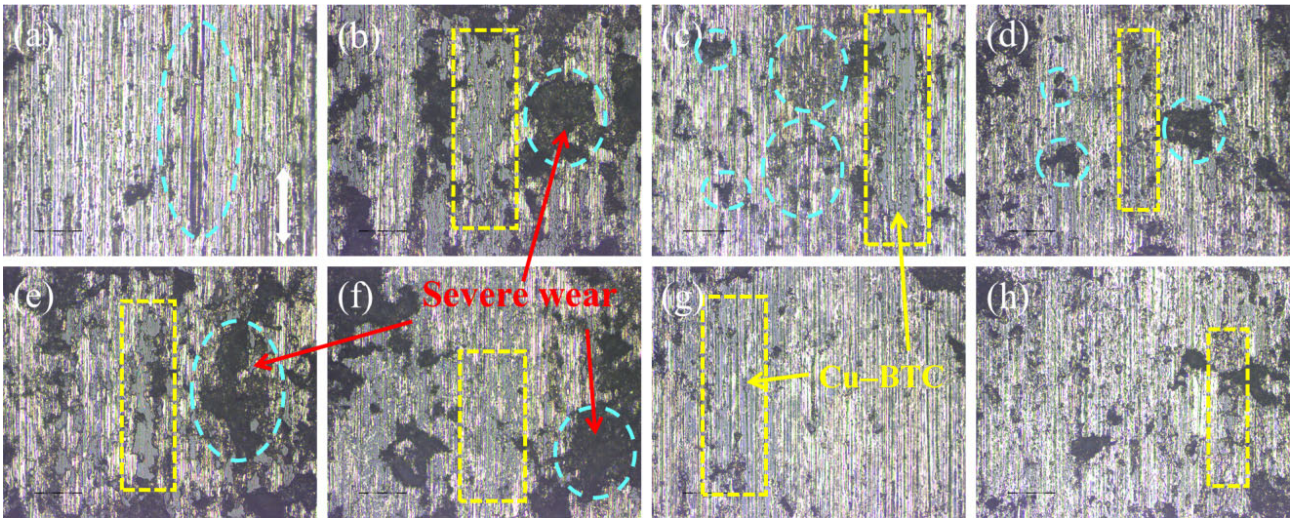

Fig. 14 Worn surfaces of (a) nothing added and (b) Cu–BTC, (c) C6@Cu–BTC, (d) C7@Cu–BTC, (e) C8@Cu–BTC, (f) C9@Cu–BTC, (g) C10@Cu–BTC, and (h) C11@Cu–BTC added.

References

[1] Millward A R, Yaghi O M. Metal–organic frameworks with exceptionally high capacity for storage of carbon dioxide at room temperature. *J Am Chem Soc* **127**(51): 17998–17999 (2005)

[2] Férey G. Microporous solids: From organically templated inorganic skeletons to hybrid frameworks… Ecumenism in chemistry. *Chem Mater* **13**(10): 3084–3098 (2001)

[3] Batten S R. Coordination polymers. *Curr Opin Solid St M* **5**(2–3): 107–114 (2001)

[4] Rao C N R, Natarajan S, Vaidhyanathan R. Metal carboxylates with open architectures. *Angew Chem Int Ed* **43**(12): 1466–1496 (2004)

[5] Chae H K, Siberio-Pérez D Y, Kim J, Go Y, Eddaoudi M, Matzger A J, O'Keeffe M, Yaghi O M. A route to high surface area, porosity and inclusion of large molecules in crystals. *Nature* **427**(6974): 523–527 (2004)

[6] Rowsell J L C, Yaghi O M. Strategies for hydrogen storage in metal–organic frameworks. *Angew Chem Int Ed* **44**(30): 4670–4679 (2005)

[7] Bauer S, Serre C, Devic T, Horcajada P, Marrot J, Férey G, Stock N. High-throughput assisted rationalization of the formation of metal organic frameworks in the iron(III) aminoterephthalate solvothermal system. *Inorg Chem* **47**(17): 7568–7576 (2008)

[8] Evans J D, Garai B, Reinsch H, Li W J, Dissegna S, Bon V, Senkovska I, Fischer R A, Kaskel S, Janiak C, et al. Metal–organic frameworks in Germany: From synthesis to function. *Coordin Chem Rev* **380**: 378–418 (2019)

[9] Silva P, Vilela S M F, Tomé J P C, Paz F A A. Multifunctional metal–organic frameworks: From academia to industrial applications. *Chem Soc Rev* **44**(19): 6774–6803 (2015)

[10] Hashemzadeh H, Raissi H, Farzad F. Design of new materials based on functionalization of Cu–BTC for adsorption and separation of CH_4 and CO_2: GCMC and MD simulations study. *Russ J Phys Chem A+* **94**(7): 1415–1421 (2020)

[11] Horcajada P, Serre C, Vallet-Regí M, Sebban M, Taulelle F, Férey G. Metal–organic frameworks as efficient materials for drug delivery. *Angew Chem Int Ed* **45**(36): 5974–5978 (2006)

[12] Liu L, Zhang Y, Qiao Y J, Tan S C, Feng S F, Ma J, Liu Y H, Luo J B. 2D metal–organic frameworks with square grid structure: A promising new-generation superlubricating material. *Nano Today* **40**: 101262 (2021)

[13] Liu L, Wang K P, Liu Y H, Luo J B. The relationship between surface structure and super-lubrication performance based on 2D MOFs. *Appl Mater Today* **26**: 101382 (2022)

[14] Zhang G L, Xie G X, Si L N, Wen S Z, Guo D. Ultralow friction self-lubricating nanocomposites with mesoporous metal–organic frameworks as smart nanocontainers for lubricants. *ACS Appl Mater Interfaces* **9**(43): 38146–38152 (2017)

[15] Fan X Q, Wang L P. High-performance lubricant additives based on modified graphene oxide by ionic liquids. *J Colloid Interf Sci* **452**: 98–108 (2015)

[16] Choudhary S, Mungse H P, Khatri O P. Dispersion of alkylated graphene in organic solvents and its potential for lubrication applications. *J Mater Chem* **22**(39): 21032–21039 (2012)

[17] Zhang W, Zhou M, Zhu H W, Tian Y, Wang K L, Wei J Q, Ji F, Li X, Li Z, Zhang P, et al. Tribological properties of oleic acid-modified graphene as lubricant oil additives. *J Phys D Appl Phys* **44**(20): 205303 (2011)

[18] Donnet C, Erdemir A. Historical developments and new trends in tribological and solid lubricant coatings. *Surf Coat Technol* **180–181**: 76–84 (2004)

[19] Erdemir A. Review of engineered tribological interfaces for improved boundary lubrication. *Tribol Int* **38**(3): 249–256 (2005)

[20] De Mello J D B, Binder C, Hammes G, Binder R, Klein A N. Tribological behaviour of sintered iron based self-lubricating composites. *Friction* **5**(3): 285–307 (2017)

[21] Pan S H, Jin K Y, Wang T L, Zhang Z N, Zheng L, Umehara N. Metal matrix nanocomposites in tribology: Manufacturing, performance, and mechanisms. *Friction* **10**(10): 1596–1634 (2022)

[22] Chui S S Y, Lo S M F, Charmant J P H, Orpen A G, Williams I D. A chemically functionalizable nanoporous material $[Cu_3(TMA)_2(H_2O)_3]_n$. *Science* **283**(5405): 1148–1150 (1999)

[23] Vishnyakov A, Ravikovitch P I, Neimark A V, Bülow M, Wang Q M. Nanopore structure and sorption properties of Cu–BTC metal–organic framework. *Nano Lett* **3**(6): 713–718 (2003)

[24] Martín-Calvo A, García-Pérez E, Castillo J M, Calero S. Molecular simulations for adsorption and separation of natural gas in IRMOF-1 and Cu–BTC metal–organic frameworks. *Phys Chem Chem Phys* **10**(47): 7085–7091 (2008)

[25] Wehring M, Gascon J, Dubbeldam D, Kapteijn F, Snurr R Q, Stallmach F. Self-diffusion studies in CuBTC by PFG NMR and MD simulations. *J Phys Chem C* **114**(23): 10527–10534 (2010)

[26] Liu J C, Culp J T, Natesakhawat S, Bockrath B C, Zande B, Sankar S G, Garberoglio G, Johnson J K. Experimental and theoretical studies of gas adsorption in $Cu_3(BTC)_2$: An effective activation procedure. *J Phys Chem C* **111**(26): 9305–9313 (2007)

[27] Mueller U, Schubert M, Teich F, Puetter H, Schierle-Arndt K, Pastré J. Metal–organic frameworks—Prospective industrial applications. *J Mater Chem* **16**(7): 626–636 (2006)

[28] Pan L, Olson D H, Ciemnolonski L R, Heddy R, Li J. Separation of hydrocarbons with a microporous metal–organic framework. *Angew Chem Int Ed* **45**(4): 616–619 (2006)

[29] Klein N, Henschel A, Kaskel S. n-butane adsorption on $Cu_3(BTC)_2$ and MIL-101. *Micropor Mesopor Mat* **129**(1–2): 238–242 (2010)

[30] Lamia N, Jorge M, Granato M A, Paz F A A, Chevreau H, Rodrigues A E. Adsorption of propane, propylene and isobutane on a metal–organic framework: Molecular simulation and experiment. *Chem Eng Sci* **64**(14): 3246–3259 (2009)

[31] Jorge M, Lamia N, Rodrigues A E. Molecular simulation of propane/propylene separation on the metal–organic framework CuBTC. *Colloid Surface A* **357**(1–3): 27–34 (2010)

[32] Rubeš M, Wiersum A D, Llewellyn P L, Grajciar L, Bludský O, Nachtigall P. Adsorption of propane and propylene on CuBTC metal–organic framework: Combined theoretical and experimental investigation. *J Phys Chem C* **117**(21): 11159–11167 (2013)

[33] Van Assche T R C, Duerinck T, Gutiérrez Sevillano J J, Calero S, Baron G V, Denayer J F M. High adsorption capacities and two-step adsorption of polar adsorbates on copper–benzene-1,3,5-tricarboxylate metal–organic framework. *J Phys Chem C* **117**(35): 18100–18111 (2013)

[34] Luna-Triguero A, Vicent-Luna J M, Gómez-Álvarez P, Calero S. Olefin/paraffin separation in open metal site Cu–BTC metal–organic framework. *J Phys Chem C* **121**(5): 3126–3132 (2017)

[35] Chmelik C, Kärger J, Wiebcke M, Caro J, van Baten J M, Krishna R. Adsorption and diffusion of alkanes in CuBTC crystals investigated using infra-red microscopy and molecular simulations. *Micropor Mesopor Mat* **117**(1–2): 22–32 (2009)

[36] Kulkarni A R, Sholl D S. Screening of copper open metal site MOFs for olefin/paraffin separations using DFT-derived force fields. *J Phys Chem C* **120**(40): 23044–23054 (2016)

[37] Dubbeldam D, Calero S, Ellis D E, Snurr R Q. RASPA: Molecular simulation software for adsorption and diffusion in flexible nanoporous materials. *Mol Simulat* **42**(2): 81–101 (2016)

Xiao YANG. He received his bachelor's and Ph.D. degrees in solid mechanics from Yanshan University, China, in 2011 and 2018, respectively. From 2014 to 2016, he worked at Uppsala University, Sweden, for cooperation research funded by China Scholarship Council (CSC). He also worked as a postdoc at State Key Laboratory of Tribology, Tsinghua University, China, from 2018 to 2020. He joined School of Mechanical Engineering, Yanshan University, China, as a lecture in 2020. His research areas cover the tribology of self-lubricating composite, self-lubricating joint bearing, and MOFs. He also interests on the application of machine learning on the tribology study. He has published more than 20 referred papers in the international journals.

Yunbo WANG. He received his bachelor's degree in mechanical design & manufacturing and their automation in 2021 from Shenyang University of Chemical Technology, China. After then, he has been a master's student in Key Laboratory of Self-Lubricating Spherical Plain Bearing Technology, Yanshan University, China. His research interests include adsorption and lubrication performance of flexible MOFs.

Weihua CAO. She received his bachelor's degree in engineering in mechanical design manufacturing and automation in 2020 from Yanshan University, China. After then, she has been studied for her Ph.D. degree in Key Laboratory of Self-Lubricating Spherical Plain Bearing Technology, Yanshan University, China. Her research interests include tribological and wear properties of polymer-based self-lubricating materials.

Guoxin XIE. He received his Ph.D. degree at Tsinghua University, China, in 2010, majoring in mechanical engineering. After that, he spent two years at State Key Laboratory of Tribology, Tsinghua University, China, for postdoctoral research. From 2012 to 2014, he worked at Royal Institute of Technology (KTH), Sweden, for another two-year postdoctoral research. Since 2014, he has worked at Tsinghua University, China, as an associate professor. His research interests include intelligent self-lubrication and electric contact lubrication. He has published more than 50 referred papers in the international journals. He won several important academic awards, such as Chinese Thousands of Young Talents, the Excellent Doctoral Dissertation Award of China, and Ragnar Holm Plaque from KTH, Sweden.